Electrical properties of indium selenide single crystals

C. De Blasi, G. Micocci, A. Rizzo, and A. Tepore
Dipartimento di Fisica, Università di Lecce, I-73100 Lecce, Italy,
and Gruppo Nazionale di Struttura della Materia, Consiglio Nazionale delle Ricerche, Lecce, Italy
(Received 30 April 1982)

Resistivity, Hall-effect, and space-charge—limited—current (SCLC) measurements were performed on InSe single crystals grown by the Bridgman-Stockbarger method. The electrical properties of the investigated samples are dominated by two donor centers at 0.10 and 0.34 eV. The latter donor influences the SCLC at room temperature. The conduction-band density-of-states effective mass was estimated to be $0.12m_0$. From the analysis of Hall-mobility data, carried out according to Schmid's model, an optical-phonon energy $\hbar\omega_f = 0.022$ eV and the coupling constant $g \simeq 0.5$ were found.

I. INTRODUCTION

Considerable attention has been devoted by various authors[1–4] to the study of the optical properties and to establishing the electronic structure of InSe single crystals. The electrical properties,[5–9] on the contrary, have been less extensively studied and this makes technical applications of InSe very difficult. In fact, it is known that semiconductor applications are governed by the electrical properties, which in turn are strongly influenced by the presence of energy levels, in the forbidden gap, arising from chemical impurities and/or structural defects.

In previous works[10,11] we reported systematic investigations of trapping-center parameters which were carried out by measurements of the thermally stimulated current (TSC) and of thermal quenching (TQ) of photoconductivity. We found three levels, located at 0.06, 0.16, and 0.34 eV below the conduction band. Their capture cross sections were found to be 1.5×10^{-23}, 9.2×10^{-21}, and 3.5×10^{-19} cm^2, respectively, and their concentrations 1.9×10^{17}, 2.3×10^{16}, and 4.2×10^{16} cm^{-3}, respectively. Moreover, a 0.20-eV center above the valence band was found to be responsible for a strong quenching of photoconductivity at low temperatures.

In the present paper we describe and analyze resisitivity, Hall-effect, and space-charge—limited—current (SCLC) measurements, performed on InSe single crystals over the temperature range 100—300 K. From the analysis of the experimental data the energies and the concentrations of the dominant donor levels were obtained, together with an estimate of the density-of-state effective mass of the conduction band. Finally, Hall-mobility results were analyzed according to a theoretical three-dimensional model proposed by Schmid.[12]

II. EXPERIMENTAL PROCEDURES

The samples analyzed in the present work were gently cleaved from single-crystal ingots of InSe obtained by the Bridgman-Stockbarger method, starting from an indium-rich liquid phase in the ratio 52-at.% indium and 48-at.% selenium. Details of the experimental equipment and procedures for crystal growth were reported elsewhere, together with some investigations on crystal structure.[13] Indium contacts were thermally evaporated in vacuum, and subsequently the samples were heated at 300 °C under an N_2 atmosphere. Contacts were checked to be Ohmic at low voltages with a curve tracer Telequipment CT71.

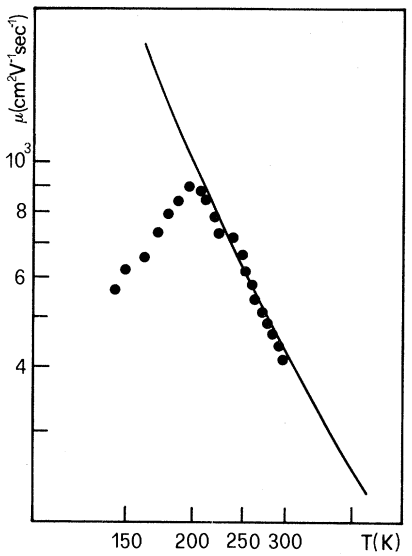

FIG. 1. Electron Hall mobility as a function of temperature for sample B_5 of InSe. Solid line is the best fit obtained with Schmid's model.

Resistivity and SCLC measurements were made in a Displex CSA-202 cryogenic refrigeration system to allow temperature ranging between 10 and 300 K. Hall-effect measurements were carried out by means of the Van der Pauw method[14] over the range of temperature between 100 and 300 K in order to obtain information about the resistivity and mobility thermal behavior. The magnetic field was about 18 kG, and the current flow was along the layers. In order to avoid thermogalvanomagnetic effects, several measurements were carried out for temperature values, by making all possible contact combinations and reversing the directions of both the current and the magnetic field. All the samples investigated turned out to be n type in the whole temperature range.

The I-V characteristics were measured at different temperatures on samples with thicknesses ranging from 50 to 150 μm and a contact area of 9 mm^2; the current flow was along the c axis. They turned out to be generally the same in all the samples investigated. For each sample the measurements were always carried out by reversing the polarity of the contacts. No appreciable differences were observed.

III. RESULTS AND DISCUSSION

A. Hall-effect results

Figure 1 shows typical behavior of the Hall mobility as a function of temperature for an InSe sample. As may be seen, at low temperature the mobility increases with temperature according to the law

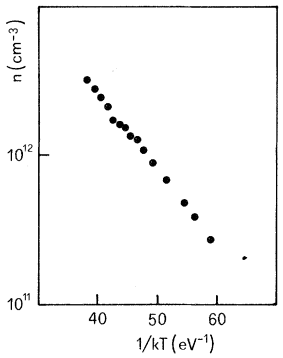

FIG. 2. Typical behavior of electron concentration n as a function of temperature.

$\mu \sim T^{3/2}$. Such a behavior is characteristic of a scattering mechanism of charge carriers with ionized impurities, which we believe to be taking place in our InSe crystals in the temperature range indicated. In the higher-temperature range ($T > 190$ K), the mobility decreases according to the law $\mu \sim T^{-2}$. This dependence indicates that an electron-lattice scattering mechanism is responsible for the mobility behavior in the high-temperature range. In this range the mobility is most likely governed by a short-range interaction with a homopolar optical phonon polarized normally to the layers, as for GaSe.[15] Unfortunately, the temperature range is not large enough to quite verify this hypothesis. According to the theoretical model proposed by Schmid,[12] the reciprocal-lifetime phonon emission and absorption are, respectively,

$$\tau_+^{-1} = \begin{cases} 0, & E < \hbar\omega_f \\ 2g^2\hbar^{-1}(n'+1)(\hbar\omega_f)^{1/2}(E-\hbar\omega_f)^{1/2}, & \text{otherwise} \end{cases} , \tag{1}$$

and

$$\tau_-^{-1} = 2g^2\hbar^{-1}n'(\hbar\omega_f)^{1/2}(E+\hbar\omega_f)^{1/2} ,$$

where $E=\hbar^2k^2/2m_e^*$ is the energy of a nearly free electron (m_e^* is the density-of-states effective mass), $\hbar\omega_f$ is the energy of the optical phonons, and n' is the number of phonons. The coupling constant g for the interband interactions of three-dimensional carriers with the homopolar optical-phonon branch is given by

$$g^2 = \frac{\epsilon^{*2}m_e^*}{2\sqrt{2}\pi\hbar MN(\hbar\omega_f)^{3/2}} , \tag{2}$$

where M is a reduced ionic mass, N is the number of cells per unit volume, and ϵ^* is the deformation potential for unit displacement for the conduction band with respect to the normal coordinate of the involved phonon. The electron drift mobility along the layers is therefore

$$\mu_{e\perp} = \frac{4e}{3\sqrt{\pi}m_{e\perp}} \int_0^\infty \tau(u)u^{3/2}\exp(-u)du , \tag{3}$$

where $u=E/kT$, $\tau=1/(\tau_+^{-1}+\tau_-^{-1})$, and $m_{e\perp}$ is the electron conduction mass along the layers. We have fitted the experimental data using Eq. (3) by assuming as adjustable parameters the phonon energy ($\hbar\omega_f$) and the coupling constant g. In this fit, the ratio of Hall effect to drift mobility was taken equal to 1. As is known, this is correct at low temperature, the limiting value at high temperature being $3\pi/8$, so that it may be considered as a constant for the purpose of comparison with experiment. The solid curve in Fig. 2 represents the best fit obtained by using the χ^2 method with a suitable high-convergence minimization procedure. The error in the experimental data was estimated to be 20%.

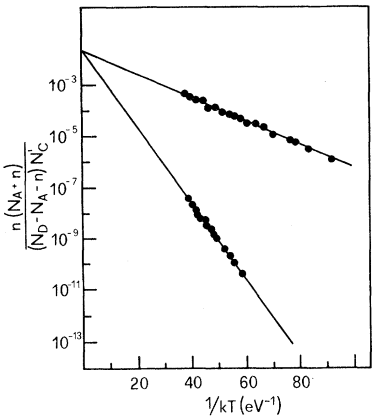

FIG. 3. Single-donor—single-acceptor model analysis of the experimental data obtained from samples A and B of InSe vs $1/kT$. Solid lines represent the computer best fit with the χ^2 method.

One can note that there is a very good agreement between theoretical and experimental behavior in the temperature range 200—300 K. The obtained values of parameters are $\hbar\omega_f = 0.022$ eV and $g = 0.5$. A similar g value has been obtained by optical measurements.[3] On the contrary, a comparison with existing results obtained on InSe with electrical measurements is not possible, since a two-dimensional model has been previously used[6] for the analysis instead of a three-dimensional one, which at least for GaSe (Ref. 16) and GaS (Ref. 17) seems more adequate.

A typical behavior of electron concentration n as a function of $1/kT$ is shown in Fig. 2. It was determined from the Hall coefficient with the use of the relation $n = r/(eR_H)$ with the Hall factor $r = 1$. The analysis of experimental data was carried out by the single-donor—single-acceptor model. According to this model, one assumes that the crystals contain a single set of donor levels of concentration N_D and ionization energy E_D and a single set of compensating acceptors of density N_A; thus, assuming the top of the valence band as the zero of energy, axis pointing to the bottom of the conduction band E_c, the following expression may be obtained from the neutrality condition for the partly compensated impurity level:

$$n + N_A = \frac{N_D}{1 + \beta \exp(\mu + E_D/kT)} , \tag{4}$$

TABLE I. Parameter values obtained from the single-donor—single-acceptor analysis shown in Fig. 3.

Samples	$N_D - N_A$	$K = N_A/N_D$	E_D (eV)	m_e^*/m_0
A	4.5×10^{16}	0.99	0.10	0.12
B	1.4×10^{16}	0.026	0.34	0.12

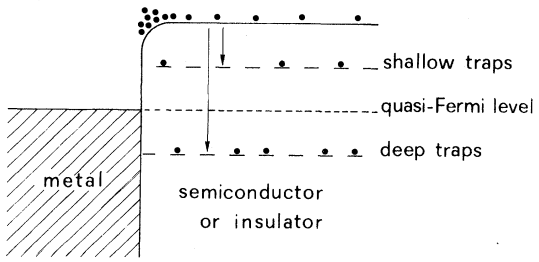

FIG. 4. Schematic energy-level diagrams for electrons injecting from an electron Ohmic contact to a semiconductor (or an insulator) with shallow and deep electron traps.

where $\mu = (F - E_c)/kT$ is the reduced Fermi-level energy and β is the multiplicity of the donor ground state including spin degeneracy. Assuming the charge carrier to be nondegenerate, the expression $\exp\mu$ can be replaced in Eq. (4) by n/N_c (where N_c is the effective density of states in the conduction band), and the following relation is obtained:

$$\frac{n(N_A+n)}{(N_D-N_A-n)N_c'} = \frac{1}{\beta}\left[\frac{m_e^*}{m_0}\right]^{3/2} \exp\left[-\frac{E_D}{kT}\right] , \tag{5}$$

with $N_c' = 2(\pi m_0 kT/h^2)^{3/2}$ and m_0 the free-electron mass.

To determine the activation energy of the donors from the experimental data, the usual curve-fitting procedure was used. The logarithm of the left-hand side of Eq. (2) against $1/kT$ was plotted with the use of $(N_D - N_A)$, $K = N_A/N_D$, and E_D as parameters. This plot results in a straight line only for the

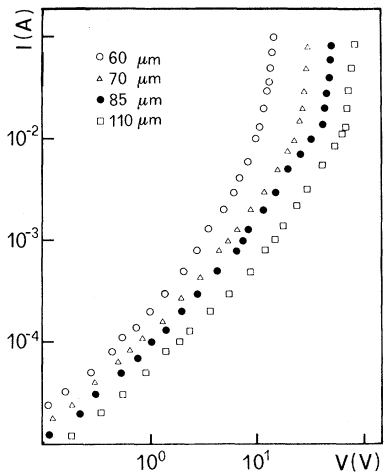

FIG. 5. Steady-state I-V characteristics at room temperature of four samples of InSe cleaved from different parts of the same ingot.

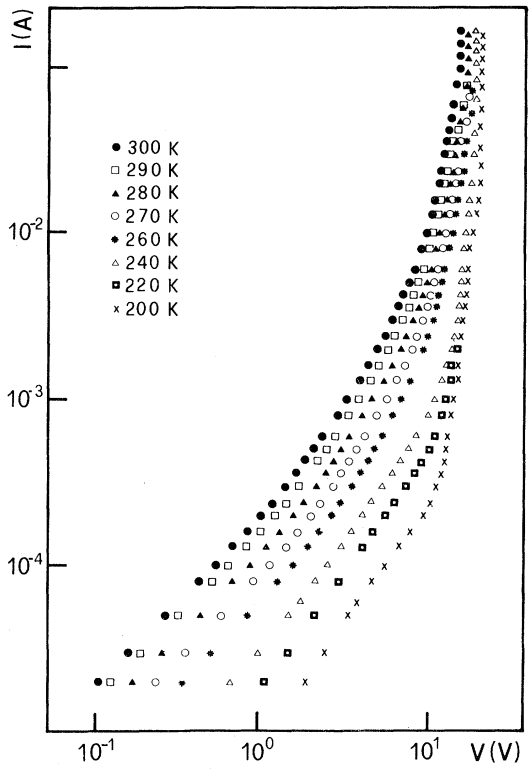

FIG. 6. Steady-state *I-V* characteristics for sample A_{20} at various temperatures.

correct values of $(N_D - N_A)$ and K. Then the slope allows the determinations of E_D and the intercept at $1/kT=0$ gives $\beta^{-1}\,(m_e^*/m_0)^{3/2}$. In Fig. 3 the plots for two samples, labeled A and B, respectively, with the best fit of the parameters, are presented. Figure 3 shows that the experimental points do correspond closely to straight lines; from the slopes two ionization energies at 0.10 and 0.34 eV are found. The intercepts at $1/kT=0$ are the same for the two samples, giving a ratio $m_e^*/m_0=0.12$. Table I reports the average values of N_D-N_A, K, E_D, and m_e^*/m_0 for the two samples.

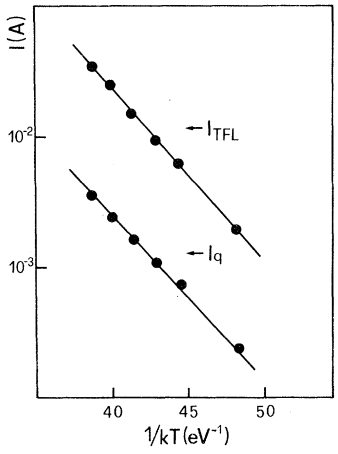

FIG. 7. Plot of I_q and I_{TFL} vs $1/kT$ for sample A_{20}.

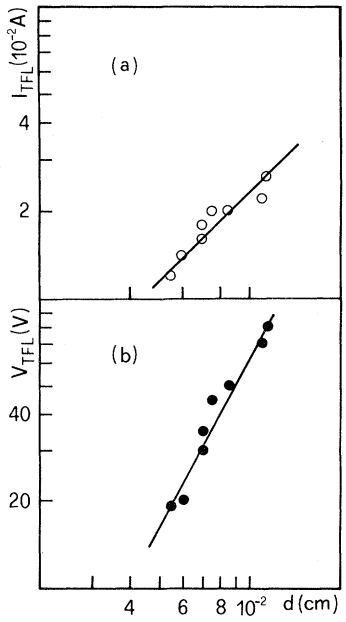

FIG. 8. (a) I_{TFL} dependence on the electrode spacing for several samples. An average linear dependence is indicated. (b) V_{TFL} dependence on the electrode spacing for the same samples as in (a). An average quadratic dependence is indicated.

B. Space-charge–limited–current results

It is known that once the electron injection takes place from the metal to the conduction band of a crystal through an Ohmic contact (Fig. 4), the

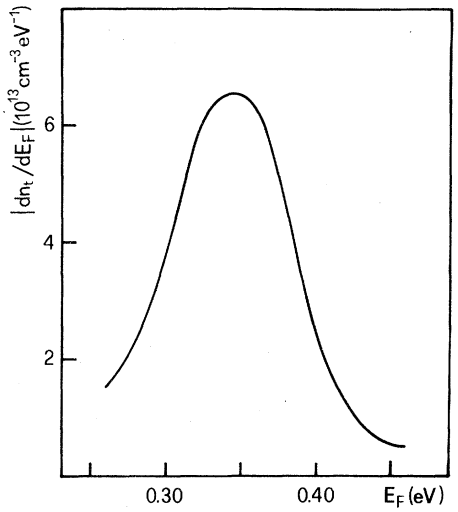

FIG. 9. Plot of $|dn_t/dE_F|$ vs energy E_F of the quasi-Fermi-level for sample A_{21} at room temperature.

behavior of the injected carriers and hence the current is controlled by the properties of the material in which the carriers are flowing. In particular, the presence of the traps created by defects present in the crystals will capture and thereby immobilize a portion of the injected carriers, thus controlling the carrier flow and determining the actual form of the current-voltage characteristics.

Experience indicates that I-V characteristics are strongly dependent on the concentration and the distribution function of traps inside the specimen. Thus their study can be a powerful method for the determination of the properties of defects in the materials.

Figure 5 shows the room temperature I-V characteristics of four InSe samples cleaved from different parts of the same ingot. No difference exists in the form of the curves; they differ only in the value of the current at a given voltage, due to different sample thicknesses. The analysis of experimental data was carried out according to the Lampert model.[18] By assuming a discrete shallow trapping level at energy E_T below the conduction-band edge, and of concentration N_T, this model predicts I-V characteristics similar to the experimental ones reported here. According to the theory, the I-V characteristics consist of an Ohmic region at low voltages, followed by a quadratic region in which the "modified Child's law" holds:

$$J_q=\tfrac{9}{8}\epsilon\mu_e\Theta(V^2/d^3)\ , \tag{6}$$

where J_q is the current density, ϵ is the static dielectric constant, μ_e is the electron mobility parallel to the c axis, V is the applied voltage, and d is the distance between the electrodes. Θ is the ratio between the free-electron concentration n and the trapped electron concentration n_t, and is written

$$\Theta=n/n_t=(N_c/\beta N_T)\exp(-E_T/kT)\ . \tag{7}$$

After the quadratic region, the current rises very steeply, starting from the voltage value V_{TFL} and the current value I_{TFL} for which complete trap filling occurs (trap filled limit).

In particular,

$$V_{\mathrm{TFL}}=eN_Td^2/2\epsilon \tag{8}$$

and

$$J_{\mathrm{TFL}}=\frac{e^2d\mu_eN_TN_c}{\beta\epsilon}\exp\left[-\frac{E_T}{kT}\right]\ . \tag{9}$$

From the previous relations one can extract N_T from the experimental value of V_{TFL} and E_T from the I_{TFL} value or from Eq. (7). Note that information about μ_e and N_c must be available to determine E_T.

A more reliable technique for obtaining E_T is to measure the J_{TFL} or J_q (at a fixed voltage) as a function of temperature. Then the resultant plot of $\ln J_{\mathrm{TFL}}$ vs $1/kT$ or $\ln J_q$ vs $1/kT$ will be a straight line whose slope is E_T.

Figure 6 shows a series of I-V characteristics of the sample A_{20} obtained at different temperatures in the range 200—300 K. From these values, $\ln I_q$ (at 6 V) and $\ln I_{\mathrm{TFL}}$ are plotted in Fig. 7 as a function of $1/kT$, from which an energy $E_T=0.32$ eV is obtained. As a comment on Fig. 6 one can note that the quadratic section length becomes shorter and shorter when decreasing the temperature; at near 200 K it is absent. This behavior indicates that the Fermi level now lies above the traps.

According to Eqs. 8 and 9, V_{TFL} should be proportional to the square of the sample thickness d^2, while J_{TFL} is a linear function of the thickness d. This is checked in Fig. 8. The fluctuations are clearly due to errors in thickness measurements and variations in trap concentration from sample to sample, but the overall agreement with these predictions is good.

The I-V characteristics also have been analyzed with the use of the method reported by Manfredotti *et al.*[19] By this method it is possible to obtain the parameters of the traps directly from I-V curves, by calculating the derivative of electron density at the anode as a function of the energy of the quasi-Fermi-level E_F. With discrete levels the derivative dn_t/dE_F has its maximum for

$$E_{F\max}=E_T+kT\ln\beta\ , \tag{10}$$

with the value

$$\left[\frac{dn_t}{dE_F}\right]_{E_{F\max}}=\frac{N_T}{4kT}\ . \tag{11}$$

Moreover, the curve dn_t/dE_F is approximately symmetric around its maximum and its full width at half maximum is about $3.5kT$. An example of such an analysis is shown in Fig. 9 for the A_{21} sample, where one obtains from Eq. (10) an energy depth of $E_T=0.32$ eV and a density $N_T=6.5\times10^{12}$ cm^{-3} from Eq. (11).

The results obtained by the I-V measurements analysis carried out with two previous methods for eight samples cleaved from different parts of the same ingot are presented in Table II. Very good agreement between the values obtained by the two methods is evident. One can also observe the quite small fluctuations among the measurements on the various sample. This provides evidence for the excellence of the methods of analysis and also for the electrical homogeneity of the ingot used.

TABLE II. Energies E_T referred to the conduction band and density of traps N_T as derived from the analysis of the I-V characteristics with the use of Lampert's model and the method proposed by Manfredotti *et al.* (Ref. 19), respectively.

	Method			
	Lampert (Ref. 18)		Manfredotti *et al.* (Ref. 19)	
Samples	E_T (eV)	N_T (10^{12} cm^{-3})	E_T (eV)	N_T (10^{12} cm^{-3})
A_{12}	0.33	8.0	0.34	6.9
A_{13}	0.32	4.5	0.32	3.6
A_{14}	0.33	6.9	0.33	4.9
A_{15}	0.33	6.1	0.34	5.4
A_{17}	0.33	6.1	0.33	5.2
A_{18}	0.33	5.8	0.32	4.6
A_{20}	0.32	5.5	0.32	3.3
A_{21}	0.33	7.1	0.32	6.5

IV. CONCLUSIONS

Summarizing, the following conclusions can be drawn:

(i) As in other layer compounds, the short-range interaction with the homopolar optical phonon is the dominant scattering mechanism limiting the Hall mobility of InSe crystals at higher temperatures. Assuming a three-dimensional conduction band, a phonon energy of around 0.022 eV and coupling constant $g \simeq 0.5$ are calculated.

(ii) At lower temperatures the mobility behavior is consistent with an ionized-impurity scattering mechanism.

(iii) Two donor levels exist at about 0.10 and 0.34 eV below the conduction band.

(iv) The 0.34-eV donor, if partially compensated, gives rise to an electron trapping center that influences the SCLC at room temperature. This conclusion is supported by the results of the systematic analysis of the electron trapping centers, in InSe, carried out by us with photoelectronic techniques.[10,11]

ACKNOWLEDGMENTS

The authors wish to thank Professor S. Mongelli for his keen interest during the progress of this work, all the workers of Unità Gruppo Nazionale di Struttura della Materia, Consiglio Nazionale delle Ricerche of University of Bari, who have made Hall measurements possible, and Mr. G. D'Elia for the technical assistance.

[1]M. V. Andriyashik, M. Yu. Sakhnonskii, V. B. Timofees, and A. S. Yakimova, Phys. Status Solidi 28, 277 (1968).
[2]Y. Depeursinge, E. Doni, R. Girlanda, A. Baldereschi, and K. Maschke, Solid State Commun. 27, 1449 (1978).
[3]J. Camassel, P. Merle, H. Mathieu, and A. Chevy, Phys. Rev. B 17, 4718 (1978).
[4]M. Piacentini, E. Doni, R. Girlanda, V. Grasso, and A. Balzarotti, Nuovo Cimento B 54, 269 (1979).
[5]R. W. Damon and R. W. Redington, Phys. Rev. 96, 1498 (1954).
[6]S. M. Atakishiev and G. A. Akhundov, Phys. Status Solidi 32, k33 (1969).
[7]G. B. Abdullaev, M. Kh. Alieva, and A. Z. Mamedova, Phys. Status Solidi 25, 75 (1968).
[8]A. Sh. Abdinov, A. G. Kyazym-Zade, N. M. Mekhtiev, M. D. Khomutova, and A. G. Sharipov, Fiz. Tech. Poluprovodn. 10, 76 (1976) [Sov. Phys.—Semicond. 10, 44 (1976)].
[9]A. Sh. Abdinov and A. G. Kyazym-Zade, Fiz. Tech. Poluprovodn. 10, 81 (1976) [Sov. Phys.—Semicond. 10, 47 (1976)].
[10]G. Micocci, A. Rizzo, and A. Tepore (unpublished).
[11]C. De Blasi, G. Micocci, A. Rizzo, and A. Tepore (unpublished).
[12]Ph. Schmid, Nuovo Cimento B 21, 258 (1974).
[13]C. De Blasi, G. Micocci, S. Mongelli, and A. Tepore, J. Cryst. Growth 57, 482 (1982).
[14]L. J. Van der Pauw, Philips Res. Rep. 13, 1 (1958).
[15]Ph. Schmid and J. P. Voitchovsky, Phys. Status Solidi A 65, 258 (1974).
[16]C. Manfredotti, A. M. Mancini, R. Murri, A. Rizzo, and L. Vasanelli, Nuovo Cimento B 39, 257 (1977).
[17]C. Manfredotti, R. Murri, A. Rizzo, and L. Vasanelli, Solid State Commun. 19, 339 (1976).
[18]M. A. Lampert and P. Mark, *Current Injection in Solids* (Academic, New York, 1970).
[19]C. Manfredotti, C. De Blasi, S. Galassini, G. Micocci, L. Ruggiero, and A. Tepore, Phys. Status Solidi A 36, 569 (1976).